Probing strong interaction effects on quantum hall states in few-layer WSe_2 by Landau level crossing

Shuigang Xu[1 †], Liheng An [1 †], Jiangxiazi Lin[1], Zefei Wu[1], Tianyi Han[1], Gen Long[1], Yuheng He[1], Fan Zhang[2], and Ning Wang[1*]*

[1]*Department of Physics and Center for Quantum Materials, the Hong Kong University of Science and Technology, Clear Water Bay, Hong Kong, China*

[2]*Departement of Physics, the University of Texas at Dallas, Richardson, Texas 75080, USA*

†These authors contributed equally to this work.

[*]Corresponding author: phwang@ust.hk (N. W.), Zhang@utdallas.edu (F. Z.)

Abstract

Atomically thin transition metal dichalcogenides (TMDCs), such as MoS_2, WSe_2, are emerging as a new platform for exploring many-body effects, because of markedly enhanced electron-electron interactions from the reduced screening in two-dimensional limits[1, 2] and large Wigner-Seitz radius[3]. Although many-body phenomena are gradually explored in optical properties of TMDCs[4, 5, 6, 7, 8, 9, 10], the probe of interaction effects on their magneto-transport properties is limited by the sample quality. Here, we experimentally demonstrate strong Coulomb interaction effects in quantum Hall regime of few-layer WSe_2 through its quantum transport behaviour in tilted magnetic fields. The Zeeman-to-cyclotron energy ratio as well as the spin susceptibility are found to be enhanced in reduced carrier density as reflected by the Landau level crossing in titled magnetic fields. The large and tuneable Landé g factor (over 4.8 times larger than that in single-particle picture) attributed to the Coulomb exchange interactions results in the carrier-density dependent quantum Hall state sequences.

Single-particle electronic states in semiconductors are well described by conventional band theory in weakly interactional systems. However, in strongly interactional systems, the Coulomb interactions between electrons can dominate the kinetic energy. The enhanced interactions can lead to a significant renormalization of the electronic band structure and carrier-density-dependent quantum transports. In atomically thin semiconducting transition metal dichalcogenides (TMDCs), Coulomb interactions can become considerably strong because of the reduced dielectric screening in two-dimensional limits[1, 2] and large Wigner-Seitz radius[3]. Strong Coulomb interactions in TMDCs can result in new physical phenomena, such as giant bandgap renormalization[4], extraordinarily large exciton-binding energies[5, 6], negative electronic compressibility[7] as well as the presence of tightly bound trions[8], biexcitons[9] and excitonic dark states[10]. However, the role of Coulomb interactions in the quantum transport of TMDCs has not been studied experimentally, mainly because of the difficulties in achieving low-temperature Ohmic contacts for high-mobility TMDCs based devices[11]. Recent progresses in the fabrication of high-mobility TMDC devices have triggered extensive studies on the intrinsic quantum transport properties in TMDCs[12, 13, 14, 15, 16, 17]. As a matter of fact, the observations of the giant spin susceptibility in few-layer WSe_2[15] and the carrier-density-dependent quantum Hall (QH) states in monolayer and bilayer WSe_2[17] already implied the existence of many-body effects in these layered structures.

The band structures of atomically thin TMDCs are layer-dependent because of interlayer interactions[18, 19]. In monolayer and bilayer WSe_2, for example, the valence band maxima locate at K/K' valleys[20, 21] with a strong spin-orbit coupling (SOC) induced band splitting[22, 23]. Due to the strong Ising SOC effect which pins electron spins to the out-of-plane direction, the Zeeman energy (E_z) of monolayer/bilayer WSe_2 only response to the out-of-plane external magnetic fields[17, 24], which is similar to the cyclotron energy (E_c). As a result, it is difficult to determine the Zeeman-to-cyclotron energy ratio (E_z/E_c) in monolayer and bilayer WSe_2 by the traditional coincidence method in tilted magnetic fields[25, 26].

In few-layer WSe_2, the interlayer coupling changes the valence band maxima to Γ valley, where SOC is negligible. In this scenario, E_z depends on the applied total magnetic fields and the coincidence technique can be used to precisely determine E_z/E_c. Therefore, few-layer WSe_2 provides a suitable platform to investigate the Coulomb interaction modification on the QH states from the determination of E_z/E_c. One of the exciting experimental results we obtained is the carrier-density-dependent Landau level (LL) crossings in titled magnetic fields. We find that the sequences of QH states are tuneable by the carrier-density-dependent E_z/E_c, accurately revealed by the coincidence method. It is surprised to observe that the spin susceptibility in few-layer WSe_2 increases with decreasing the carrier density even in a relatively high-density regime (~ 5×10^{12} cm^{-2}), much higher than that required for detecting the electron-electron interaction effects in most two-dimensional electron gas (2DEG) systems.

The high-quality WSe_2 devices are fabricated based on the dry transfer technique reported previously[27]. Technical details about the h-BN encapsulated structure and the selective etching technique for fabricating low-temperature Ohmic contacts to WSe_2 can be found in Ref.[13, 14, 15, 28]. High work function metal Pd is used as the contact electrodes, which help us

access the Γ valley in few-layer WSe_2. The high-performance devices with a typical Hall mobility of 4500 cm^2/V s (at n=5.7×10^{12} cm^{-2}) allow us to observe the QH states at cryogenic temperatures. The typical magneto-transport at a relatively low hole density of 2.5×10^{12} cm^{-2} is shown in Fig. 1a. The hole density is determined from the slope of the Hall resistance at linear regions. Shubnikov-de Haas (SdH) oscillations in longitudinal resistance (R_{xx}) and quantized plateaux in Hall resistance (R_{xy}) are clearly visible in Fig. 1a. At n =2.5×10^{12} cm^{-2}, the quantized plateaux in R_{xy} are observed at filling factors (FFs) of $\nu = 7, 9, 11, ...$ (odd-integers) with the appearance of corresponding minima in R_{xx}. The two-fold spin degeneracy along with single valley is the characteristic of the Γ valley in WSe_2, which can be verified by comparing the total carrier density with SdH oscillation periods[15]. These odd-integer dominated QH states are similar to that reported previously[15], which is because of the special value of E_z/E_c. In the present study, we further discover that the QH state sequence varies as the hole density changes. As shown in Fig. 1b, the QH state changes to even-integer sequence at n =3.4×10^{12} cm^{-2}. Figure 1c shows R_{xx} plotted as a function of FFs at different hole densities. The FFs are calculated by $\nu = nh/eB$, where n is the carrier density, h the Planck's constant, B the magnetic field, and e the charge of an electron. At n =2.5×10^{12} cm^{-2}, the R_{xx} minima regularly appear at odd FFs, such as $\nu = 9, 11, 13, ...$, consistent with the quantized plateaux in R_{xy} in Fig. 1a. Comparatively, from n =3.4×10^{12} cm^{-2} to 4.8×10^{12} cm^{-2}, the strong R_{xx} minima occur at even FFs. Although weak R_{xx} minima can be observed at odd FFs under high B because of the Zeeman effect, the even QH states predominate in these regions. As the hole density further increases to 5.7×10^{12} cm^{-2}, the main R_{xx} minima change to odd FFs again, i.e., the QH state sequence is back to odd. The results shown in Fig. 1c indicate that the QH states vary with carrier densities. A similar phenomenon has been observed recently in monolayer and bilayer WSe_2[17], which suggests the origin is not from valley-dependent properties, such as spin splitting and valley degeneracy. In the following, we demonstrate that it is Coulomb interactions that play an important role in modifying the QH states in the Γ valley of few-layer WSe_2.

The QH state sequence in spin degenerated LL is determined by the ratio of E_z/E_c. The density-dependent QH states are originated from the competitions between E_z and E_c in various carrier densities. In the Γ valley of few-layer WSe_2, when $2j + 0.5 < E_z/E_c < 2j + 1.5$, with j being a non-negative integer, the odd-integer QH states predominate in the system. While, $2j - 0.5 < E_z/E_c < 2j + 0.5$ yields an even-integer dominated QH states. It is noteworthy that the situation is the opposite in the monolayer case because of the SOC in the valence band of K valleys[29]. In order to study how the QH states change with carrier densities, E_z/E_c should be determined at different carrier densities. Traditionally, the coincidence technique is an accurate method to measure E_z/E_c in 2DEG systems[26]. Thanks to the negligible SOC in Γ valley, this technique is executable in few-layer WSe_2. The strong spin-locking in monolayer WSe_2, however, prevents the determination of E_z/E_c through the coincidence technique[17].

We use the coincidence technique to measure the SdH oscillations of few-layer WSe_2 at 1.7 K at various tilting angles θ as shown in Fig. 2. The value of θ is calibrated by the simultaneous Hall measurements in linear regions, since the total carrier density does not

change when tilting the samples. At a tilting angle θ, the cyclotron energy $E_c = \hbar e B_\perp / m^*$, is proportional to the perpendicular component of the magnetic field ($B_\perp$), where $\hbar$ is the reduced Planck's constant and m^* is the effective mass,. While, the Zeeman energy $E_z = g^* \mu_B B_{tot}$, increases with increasing the total magnetic field B_{tot}, where $g^*$is the effective Landé g factor and μ_B is the Bohr magneton,. Therefore, when tilting B, LL crossing can be realized at the so-called coincidence angles as shown in Fig. 3c. The coincidence angles occur at $E_z/E_c = g^* m^*/2m_0 cos\theta = i$, when i takes on integer values.

Figure 2 shows R_{xx} vs $B_\perp$ at various θ for two representative hole densities of n_1=4.0×10^{12} cm^{-2} and n_2=5.7×10^{12} cm^{-2}. Both of them give significant angle-dependent SdH oscillations. For example, at n_1 the odd-integer QH states at $\nu = 15, 17, 19, ...$ become weaker and weaker, and eventually vanish as θ increases from 0° to 24.3°. At the first coincidence angle of $\theta = 24.3°$, strongest SdH minima (maxima) appear at the even- (odd-) integer states. As the angle further increases to the second coincidence angle at $\theta = 44.1°$, a phase reversal[25] in the oscillation is observed, i.e., the SdH minima (maxima) gradually become maxima (minima). Comparing the evolutions of SdH as θ at n_1 with that at n_2, we find two important features. First, the coincidence angles at n_1 and n_2 are different. At n_1=4.0×10^{12} cm^{-2}, the coincidence angles are 24.3°, 44.1° and 54.5°, while at n_2=5.7×10^{12} cm^{-2}, the coincidence angles are 28.9°, 48.2° and 57.4°. The different coincidence conditions indicate different values of E_z/E_c at different hole densities. Second, the evolutions of the QH states are different, particularly at the coincidence angles. For example, at respective first coincidence angles, for n_1, the SdH minima occur at even FFs, while for n_2, the SdH minima occur at odd FFs.

Based on the coincidence angles, we can accurately extract spin susceptibility $g^* m^*$ from the slope of linear fitting by $icos\theta = g^* m^*/2m_0$. The results shown in Fig. 3a yield $g^* m^* = 7.1m_0$ at n_1 and $g^* m^* = 5.34m_0$ at n_2. We believe that the enhanced $g^* m^*$ as the carrier density reduces is because of electron-electron interactions. The values of E_z/E_c at $\theta = 0°$ are 3.55 for n_1, and 2.67 for n_2, respectively. According to the aforementioned analysis, since $3.5 < E_z/E_c < 4.5$ for n_1, even-integer QH state sequence predominates at small B. In contrast, for n_2, $2.5 < E_z/E_c < 3.5$, odd-integer QH state sequence predominates. The experimental results shown in Fig. 1c agree fairly well with such a physical picture. Figure 3c schematically demonstrates the evolution of LL as a function of tilted angles under a constant $B_\perp$. The locations of zero tilted angle at n_1 and n_2 are marked according to the obtained E_z/E_c.

The amplitudes of SdH oscillations vary at different tilted angles. The maximum oscillation amplitudes appear at coincidence angles (Fig. 2). In fact, the angle-dependent amplitude of SdH oscillations can be described by[30, 31] $R(\theta) \propto \cos(\frac{\pi g^* m^*}{2m_0 \cos\theta})$. Using this formula, we can alternatively fit the angle-dependent amplitudes with a parameter $g^* m^*$. The fittings in Fig. 3b yield $g^* m^* = 7.08m_0$ at n_1 and $g^* m^* = 5.42m_0$ at n_2, which agree fairly well with the fitting from coincidence angles shown in Fig. 3a.

According to the obtained E_z/E_c and the demonstration in Fig. 3c, the first coincidence angle occurs at difference index i, with $i = 4$ for n_1 and $i = 3$ for n_2. The spin up states in *N*th LL are degenerate with the spin down states in (*N*+4)th LL at the first coincidence angle of n_1. Correspondingly, the spin up states in *N*th LL and spin down states in (*N*+3)th LL are degenerate for n_2. The QH states have different sequence at $i = 3$ and $i = 4$. For $i = 3$, the sequence is $\nu = 1, 2, 3, 5, 7, 9, ...$, while for $i = 4$, the sequence is $\nu = 1, 2, 3, 4, 6, 8, ...$ Figure 4a and 4b show consistent QH plateaus in R_{xy} at each first coincidence angle for n_1 and n_2.

The observed strong carrier-density-dependent spin susceptibility is one of the signatures of Coulomb interactions. In the many-body theory, exchange interactions can enhance g^*m^* with decreasing the carrier density in 2DEG systems. Usually, the strength of Coulomb interactions is determined by the ratio of the Coulomb energy and the kinetic energy. This ratio is often expressed in terms of the Wigner-Seitz radius $r_s = \frac{1}{\sqrt{\pi n} a_B^*}$, where n is the carrier density, $a_B^* = a_B \varepsilon (m_0/m^*)$ is the Bohr radius a_B corrected by the dielectric environment with dielectric constant ε. This radius represents the average inter-electron spacing and is tuneable by varying the density of an interacting system. A large r_s reflects a strong interaction occurring in the system. Because of the large m^* at the valence band of Γ valley in WSe_2 and the weak dielectric screening in the two-dimensional limit, r_s is large enough even at high carrier densities, resulting in strong interaction related effects in our samples. By taking the environmental dielectric constant of h-BN $\varepsilon = \sqrt{\varepsilon_\perp \varepsilon_\parallel} \approx 4.15$ with $\varepsilon_\perp = 2.5$ and $\varepsilon_\parallel = 6.9$ [32, 33]and the valence band effective mass at Γ valley $m^* = 0.75 m_0$ (see details in Supplementary Information), the estimated r_s is around 7.7-12.2 in the carrier density region of 2.5×10^{12} cm^{-2} to 6.2×10^{12} cm^{-2}. Typically, an electron system with $r_s \sim 10$ is considered to be a strongly correlated system, and $r_s \sim 37$ is a critical value for the Wigner crystallization in 2DEG systems[34]. In a traditional 2DEG, such as Si[35, 36], GaAs[37, 38] and AlAs[39, 40], in order to observe the interaction enhanced spin susceptibility, a much lower carrier density (typically in the order of 10^{11} cm^{-2} or even lower) has to be achieved. Our system provides an appropriate platform to study the many-body ground states in 2DEG.

Alternatively, g^*m^* can be determined by another method from magneto-transport measurements. When a magnetic field is applied in the direction parallel to the 2DEG device, Zeeman splitting induces different population of the spin-up and spin-down sub-bands. When the parallel B is above a critical value, the splitting exceeds the Fermi energy and the system is fully spin polarized. There will be a resistance kink at this state. From the onset of the kink at the critical field[37, 38] $B_p = 2\pi\hbar^2 n/\mu_B g^* m^*$, one can roughly estimate g^*m^* . However, because our system is in high carrier density region, B_p is too large to achieve in normal experimental laboratories. For example, at n_1=4.0×10^{12} cm^{-2}, by using $g^*m^* = 7.1 m_0$ (based on the coincidence method), the estimated critical field is $B_p = 46.7$ T.

In 2DEG, Coulomb interaction can enhance both m^* and g^* at a low carrier density[36, 37, 40]. To identify the main enhanced factor in spin susceptibility g^*m^* , we measure the temperature-dependent SdH oscillations at different carrier densities to extract m^*(see details in Supplementary Information). In our system, we do not observe obvious changes of m^* by

changing the carrier density from 2.8×10^{12} cm^{-2} to 6.6×10^{12} cm^{-2}. Therefore, we believe the contribution of interaction enhancement of g^*m^* is mainly from g^*. By using the measured $m^* = 0.75m_0$, we have $g^* = 9.5$ and 7.1 at n_1 and n_2, respectively. Thus, about 4.8 times enhancement in g^* over the free hole value of 2.0 in the single-particle picture is obtained for the Γ valley of WSe_2. Since the interlayer coupling influences the band structure of Γ valley[20], the values of m^* measured from different samples are slightly different[15].

In summary, we reported the carrier-density-dependent spin susceptibility at the Γ valley of WSe_2 by observing LL crossings in tilted magnetic fields. The strong electron-electron interactions enhance the spin susceptibility at low carrier densities, resulting the increased Zeeman-to-cyclotron energy ratio. As a result, the QH states show different sequences at different carrier densities. Our work suggests that the giant spin susceptibility together with strong electron-electron interactions in few-layer WSe_2 may lead to exotic QH states, such as QH ferromagnetism[41] and even-denominator fractional QH[42].

Methods

WSe_2 crystals were grown by chemical vapour transport. Few-layer WSe_2 flakes were mechanically exfoliated on SiO_2/Si substrates by the scotch tape method. The top h-BN was exfoliated on a PPMA membrane and used to pick up WSe_2 flakes. The h-BN/WSe_2 structure was then transferred onto a bottom h-BN, previously exfoliated and selected on a 300 nm SiO_2/Si substrate. The size of the WSe_2 flake was selected to make sure it can be fully encapsulated by the top and bottom h-BN sheets. The encapsulated structures allow us to safely anneal the samples at a high temperature up to 400 °C in Ar atmosphere in order to remove small bubbles. To fabricate the metal electrodes, we chose the selective etching process. Standard Hall bar device structure was patterned on a PMMA first, which was also used as the hard mask in the etching process. To expose the contact area of WSe_2, we used reactive ion etching to etch the top h-BN. It is possible to control the etching process with 40 sccm O_2 as the recipe, because the etching rate of WSe_2 is much lower than that of h-BN. Finally, Pd/Au (20/80 nm) was used as the p-type contact metal via a standard e-beam evaporation.

The transport measurements were conducted using standard lock-in techniques at 1.7 K. In order to study the quantum transport in tilted magnetic fields, we used a home-built probe with a sample stage which can be *in situ* rotated via a mechanical knob. The titled angles were internally calibrated by the Hall measurements of the sample, which guarantees their accuracy.

Acknowledgements

Financial support from the Research Grants Council of Hong Kong (Project Nos. 16302215, HKU9/CRF/13G) and technical support of the Raith-HKUST Nanotechnology Laboratory for the electron-beam lithography facility at MCPF are hereby acknowledged.

Author contributions

N.W. and S.X. conceived the projects. S.X. grew the crystal. S.X., L.A. fabricated and measured the devices. S.X., L.A., F.Z. and N.W. analysed the data. F.Z. and N.W. were the principal investigators. S.X., F.Z. and N.W. wrote the manuscript. Other authors provided technical assistances, discussions and comments.

References

1. Berkelbach TC, Hybertsen MS, Reichman DR. Theory of neutral and charged excitons in monolayer transition metal dichalcogenides. *Phys Rev B* 2013, **88**(4)**:** 045318.

2. Cudazzo P, Tokatly IV, Rubio A. Dielectric screening in two-dimensional insulators: Implications for excitonic and impurity states in graphane. *Phys Rev B* 2011, **84**(8)**:** 085406.

3. Wang Z, Shan J, Mak KF. Valley- and spin-polarized Landau levels in monolayer WSe_2. *Nat Nano* 2017, **12**(2)**:** 144-149.

4. Ugeda MM, Bradley AJ, Shi S-F, da Jornada FH, Zhang Y, Qiu DY*, et al.* Giant bandgap renormalization and excitonic effects in a monolayer transition metal dichalcogenide semiconductor. *Nat Mater* 2014, **13**(12)**:** 1091-1095.

5. He K, Kumar N, Zhao L, Wang Z, Mak KF, Zhao H*, et al.* Tightly Bound Excitons in Monolayer WSe_2. *Phys Rev Lett* 2014, **113**(2)**:** 026803.

6. Zhu B, Chen X, Cui X. Exciton Binding Energy of Monolayer WS_2. *Sci Rep* 2015, **5:** 9218.

7. Riley JM, MeevasanaW, BawdenL, AsakawaM, TakayamaT, EknapakulT*, et al.* Negative electronic compressibility and tunable spin splitting in WSe_2. *Nat Nano* 2015, **10**(12)**:** 1043-1047.

8. Mak KF, He K, Lee C, Lee GH, Hone J, Heinz TF*, et al.* Tightly bound trions in monolayer MoS_2. *Nat Mater* 2013, **12**(3)**:** 207-211.

9. You Y, Zhang X-X, Berkelbach TC, Hybertsen MS, Reichman DR, Heinz TF. Observation of biexcitons in monolayer WSe_2. *Nat Phys* 2015, **11**(6)**:** 477-481.

10. Ye Z, Cao T, O'Brien K, Zhu H, Yin X, Wang Y*, et al.* Probing excitonic dark states in single-layer tungsten disulphide. *Nature* 2014, **513**(7517)**:** 214-218.

11. Allain A, Kang J, Banerjee K, Kis A. Electrical contacts to two-dimensional semiconductors. *Nat Mater* 2015, **14**(12)**:** 1195-1205.

12. Cui X, Lee G-H, Kim YD, Arefe G, Huang PY, Lee C-H*, et al.* Multi-terminal transport measurements of MoS_2 using a van der Waals heterostructure device platform. *Nat Nano* 2015, **10**(6)**:** 534-540.

13. Xu S, Wu Z, Lu H, Han Y, Long G, Chen X*, et al.* Universal low-temperature Ohmic contacts for quantum transport in transition metal dichalcogenides. *2D Mater* 2016, **3**(2)**:** 021007.

14. Wu Z, Xu S, Lu H, Khamoshi A, Liu G-B, Han T*, et al.* Even–odd layer-dependent magnetotransport of high-mobility Q-valley electrons in transition metal disulfides. *Nat Commun* 2016, **7:** 12955.

15. Xu S, Shen J, Long G, Wu Z, Bao Z-q, Liu C-C*, et al.* Odd-Integer Quantum Hall States and Giant Spin Susceptibility in *p*-Type Few-Layer WSe_2. *Phys Rev Lett* 2017, **118**(6)**:** 067702.

16. Fallahazad B, Movva HCP, Kim K, Larentis S, Taniguchi T, Watanabe K*, et al.* Shubnikov-de Haas Oscillations of High-Mobility Holes in Monolayer and Bilayer WSe_2: Landau Level Degeneracy, Effective Mass, and Negative Compressibility. *Phys Rev Lett* 2016, **116**(8)**:** 086601.

17. Movva HCP, Fallahazad B, Kim K, Larentis S, Taniguchi T, Watanabe K*, et al.* Density-Dependent Quantum Hall States and Zeeman Splitting in Monolayer and Bilayer WSe_2. *Phys Rev Lett* 2017, **118**(24)**:** 247701.

18. Mak KF, Lee C, Hone J, Shan J, Heinz TF. Atomically Thin MoS_2: A New Direct-Gap Semiconductor. *Phys Rev Lett* 2010, **105**(13)**:** 136805.

19. Jin W, Yeh P-C, Zaki N, Zhang D, Sadowski JT, Al-Mahboob A*, et al.* Direct Measurement of the Thickness-Dependent Electronic Band Structure of MoS_2 Using Angle-Resolved Photoemission Spectroscopy. *Phys Rev Lett* 2013, **111**(10)**:** 106801.

20. Wilson NR, Nguyen PV, Seyler K, Rivera P, Marsden AJ, Laker ZPL*, et al.* Determination of band offsets, hybridization, and exciton binding in 2D semiconductor heterostructures. *Sci Adv* 2017, **3**(2)**:** e1601832.

21. Zeng H, Liu G-B, Dai J, Yan Y, Zhu B, He R*, et al.* Optical signature of symmetry variations and spin-valley coupling in atomically thin tungsten dichalcogenides. *Sci Rep* 2013, **3:** 1608.

22. Xiao D, Liu G-B, Feng W, Xu X, Yao W. Coupled Spin and Valley Physics in Monolayers of MoS_2 and Other Group-VI Dichalcogenides. *Phys Rev Lett* 2012, **108**(19)**:** 196802.

23. Zhu ZY, Cheng YC, Schwingenschlögl U. Giant spin-orbit-induced spin splitting in two-dimensional transition-metal dichalcogenide semiconductors. *Phys Rev B* 2011, **84**(15)**:** 153402.

24. Lu JM, Zheliuk O, Leermakers I, Yuan NFQ, Zeitler U, Law KT*, et al.* Evidence for two-dimensional Ising superconductivity in gated MoS_2. *Science* 2015, **350**(6266)**:** 1353.

25. Fang FF, Stiles PJ. Effects of a Tilted Magnetic Field on a Two-Dimensional Electron Gas. *Phys Rev* 1968, **174**(3)**:** 823-828.

26. Nicholas RJ, Haug RJ, Klitzing Kv, Weimann G. Exchange enhancement of the spin splitting in a GaAs-$Ga_xAl_{1-x}As$ heterojunction. *Phys Rev B* 1988, **37**(3)**:** 1294-1302.

27. Wang L, Meric I, Huang PY, Gao Q, Gao Y, Tran H*, et al.* One-Dimensional Electrical Contact to a Two-Dimensional Material. *Science* 2013, **342**(6158)**:** 614.

28. Chen X, Wu Y, Wu Z, Han Y, Xu S, Wang L*, et al.* High-quality sandwiched black phosphorus heterostructure and its quantum oscillations. *Nat Commun* 2015, **6:** 7315.

29. Li X, Zhang F, Niu Q. Unconventional Quantum Hall Effect and Tunable Spin Hall Effect in Dirac Materials: Application to an Isolated MoS_2 Trilayer. *Phys Rev Lett* 2013, **110**(6)**:** 066803.

30. Kurganova EV, van Elferen HJ, McCollam A, Ponomarenko LA, Novoselov KS, Veligura A*, et al.* Spin splitting in graphene studied by means of tilted magnetic-field experiments. *Phys Rev B* 2011, **84**(12)**:** 121407.

31. Cao Y, Mishchenko A, Yu GL, Khestanova E, Rooney AP, Prestat E*, et al.* Quality Heterostructures from Two-Dimensional Crystals Unstable in Air by Their Assembly in Inert Atmosphere. *Nano Lett* 2015, **15**(8)**:** 4914-4921.

32. Geick R, Perry CH, Rupprecht G. Normal Modes in Hexagonal Boron Nitride. *Phys Rev* 1966, **146**(2)**:** 543-547.

33. Wang Z, Mak KF, Shan J. Strongly interaction-enhanced valley magnetic response in monolayer WSe_2. *arXiv preprint* 2017**:** arXiv:1705.01078.

34. Tanatar B, Ceperley DM. Ground state of the two-dimensional electron gas. *Phys Rev B* 1989, **39**(8)**:** 5005-5016.

35. Okamoto T, Hosoya K, Kawaji S, Yagi A. Spin Degree of Freedom in a Two-Dimensional Electron Liquid. *Phys Rev Lett* 1999, **82**(19)**:** 3875-3878.

36. Pudalov VM, Gershenson ME, Kojima H, Butch N, Dizhur EM, Brunthaler G*, et al.* Low-Density Spin Susceptibility and Effective Mass of Mobile Electrons in Si Inversion Layers. *Phys Rev Lett* 2002, **88**(19)**:** 196404.

37. Tutuc E, Melinte S, Shayegan M. Spin Polarization and *g* Factor of a Dilute GaAs Two-Dimensional Electron System. *Phys Rev Lett* 2002, **88**(3)**:** 036805.

38. Zhu J, Stormer HL, Pfeiffer LN, Baldwin KW, West KW. Spin Susceptibility of an Ultra-Low-Density Two-Dimensional Electron System. *Phys Rev Lett* 2003, **90**(5)**:** 056805.

39. Shkolnikov YP, Vakili K, De Poortere EP, Shayegan M. Dependence of Spin Susceptibility of a Two-Dimensional Electron System on the Valley Degree of Freedom. *Phys Rev Lett* 2004, **92**(24)**:** 246804.

40. Padmanabhan M, Gokmen T, Bishop NC, Shayegan M. Effective Mass Suppression in Dilute, Spin-Polarized Two-Dimensional Electron Systems. *Phys Rev Lett* 2008, **101**(2)**:** 026402.

41. De Poortere EP, Tutuc E, Papadakis SJ, Shayegan M. Resistance Spikes at Transitions Between Quantum Hall Ferromagnets. *Science* 2000, **290**(5496)**:** 1546.

42. Falson J, Maryenko D, Friess B, Zhang D, Kozuka Y, Tsukazaki A*, et al.* Even-denominator fractional quantum Hall physics in ZnO. *Nat Phys* 2015, **11**(4)**:** 347-351.

Figures:

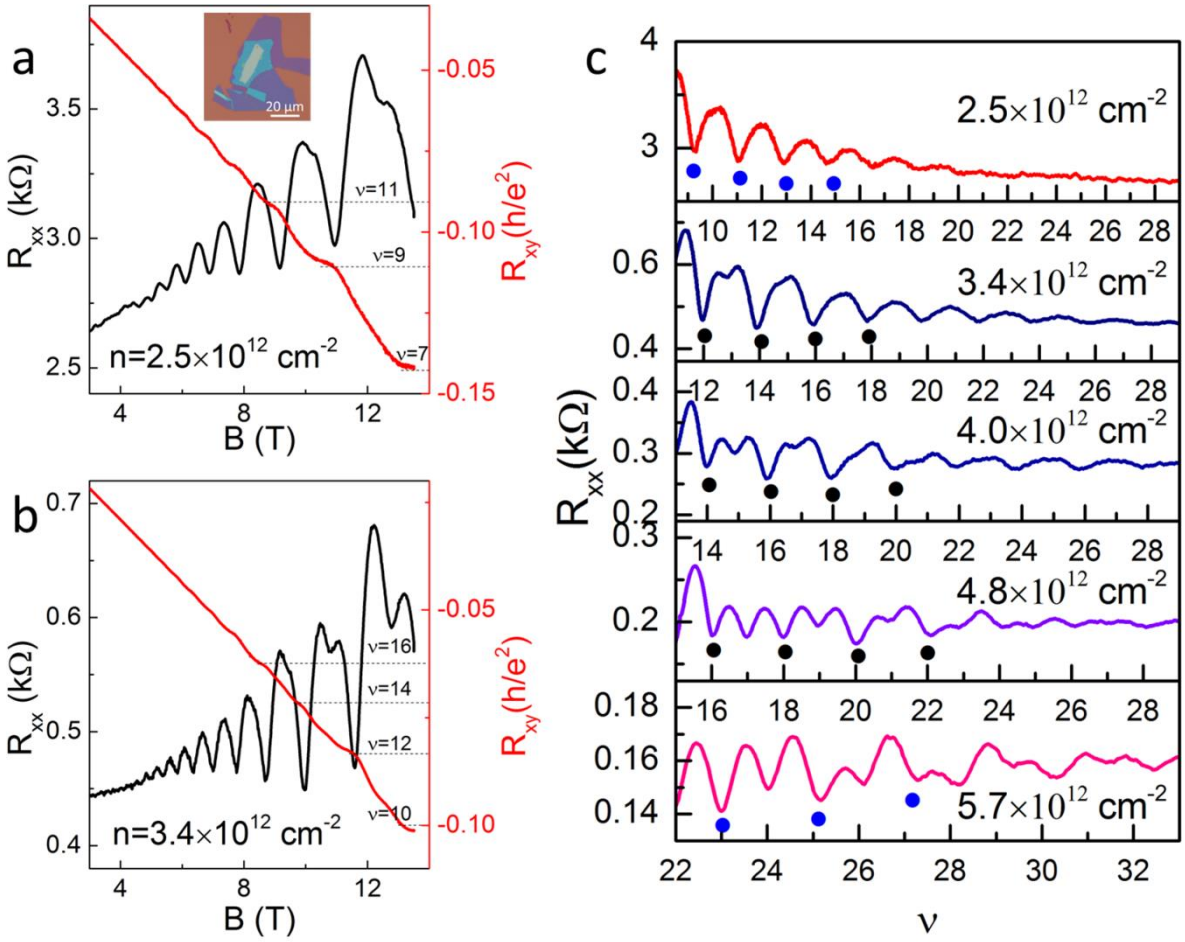

Figure 1: Quantum oscillations in various carrier densities. (**a,b**) R_{xx} and R_{xy} as a function of B at (**a**) $n = 2.5 \times 10^{12}$ cm^{-2}, (**b**) $n = 3.4 \times 10^{12}$ cm^{-2}. QH plateaux in R_{xy} are marked. The inset in (**a**) is an optical image of the h-BN encapsulated WSe_2 structure. (**c**) R_{xx} as a function of ν at various n. The FFs are calculated by $\nu = nh/eB$. The main minima are marked. The odd and even predominated QH states are distinguished by blue and black colours, respectively. All data were recorded at T=1.7 K.

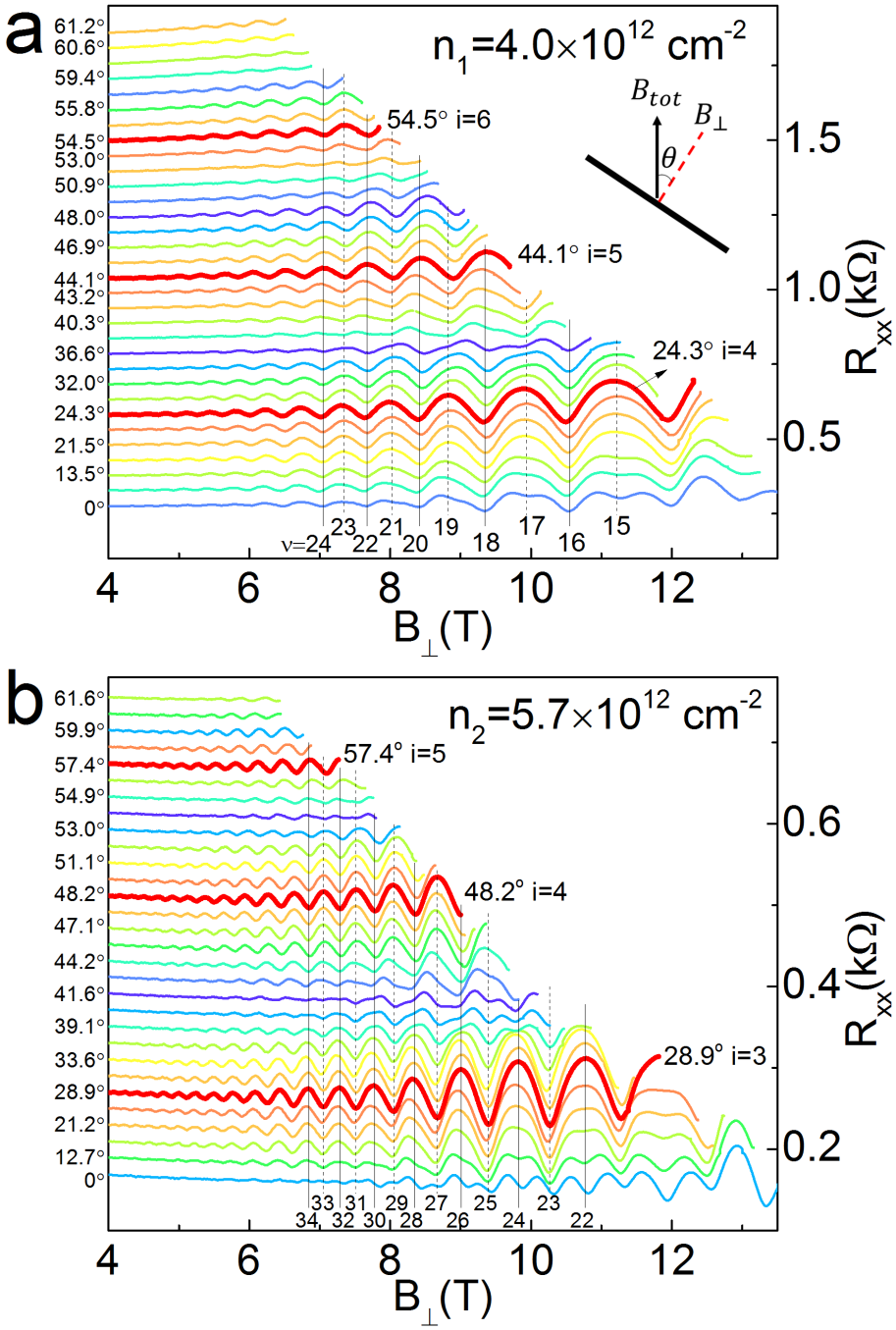

Figure 2: Carrier-density-dependent Landau level crossing in titled magnetic fields. R_{xx} as a function of $B_\perp$ at various titled angles for two representative carrier densities: (**a**) $n_1 = 4.0 \times 10^{12}$ cm^{-2}, (**b**) $n_2 = 5.7 \times 10^{12}$ cm^{-2}. The main angles are labelled in the neighbour of left axis. The curves at corresponding coincidence angles are in bold. The data at non-zero angles are vertically offset for clarity. The inset in (**a**) is the schematic of rotating angles with respect to total magnetic fields.

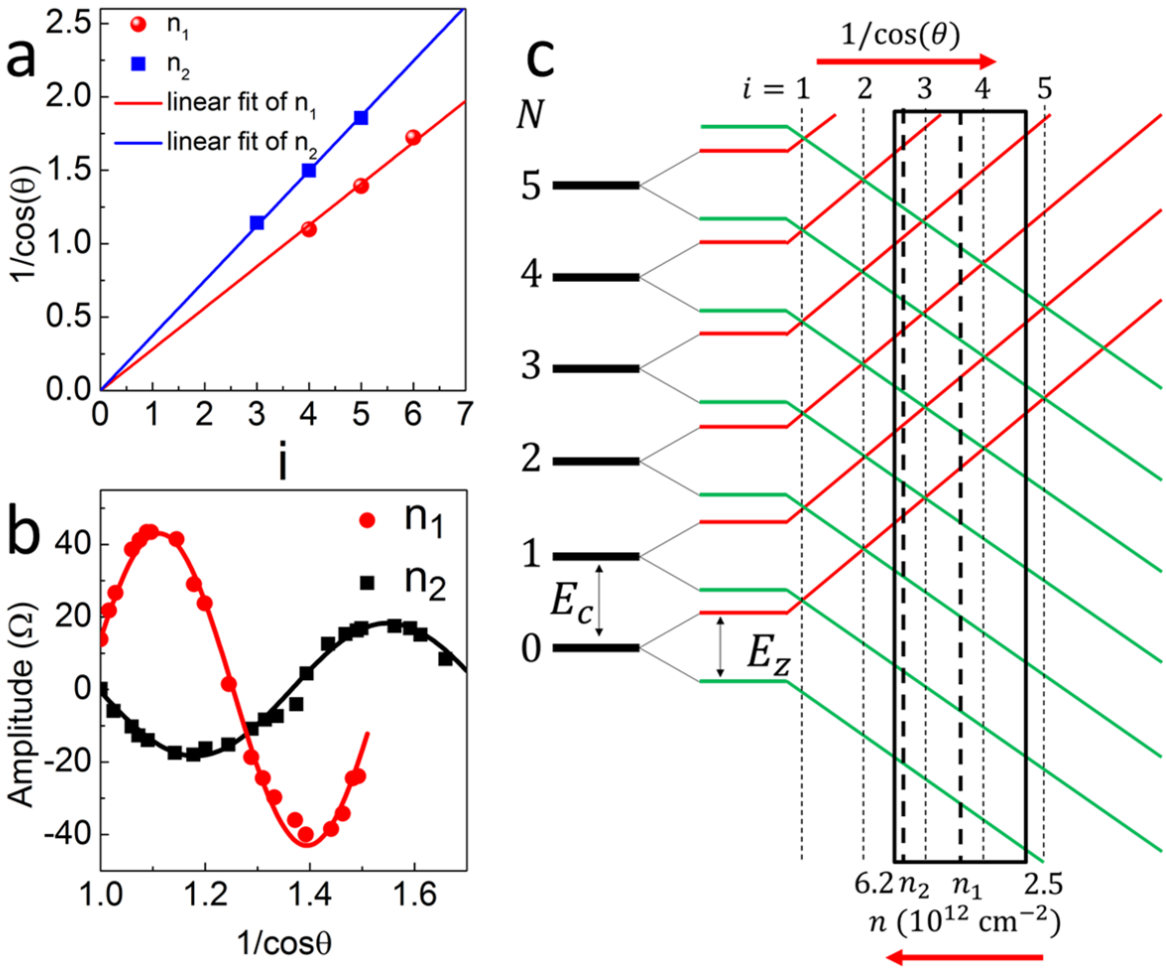

Figure 3: Determination of spin susceptibility. (**a**) $1/cos\theta$ at coincidence angles as a function of coincidence indices i for n_1 and n_2. The slopes of linear fit yields the spin susceptibility as well as E_z/E_c at $\theta = 0°$. (**b**) SdH amplitudes as a function of $1/cos\theta$ for n_1 (recorded at $\nu = 19$) and n_2(recorded at $\nu = 29$). The data were fitted with cosine functions, yielding fitting parameter of spin susceptibility g^*m^*. (**c**) Schematic diagram depicts the LL evolving with tilt angles in a tilted B and carrier densities n. Under a fixed $B_\perp$, E_c does not change, while E_z linearly increases with B_{tot} as increasing θ. Both increasing θ and decreasing n can enhance E_z/E_c. The black block illustrates the carrier density regime we can approach in our experiment for $= 0°$. The bold dashed lines mark the location of $\theta = 0°$ for n_1 and n_2.

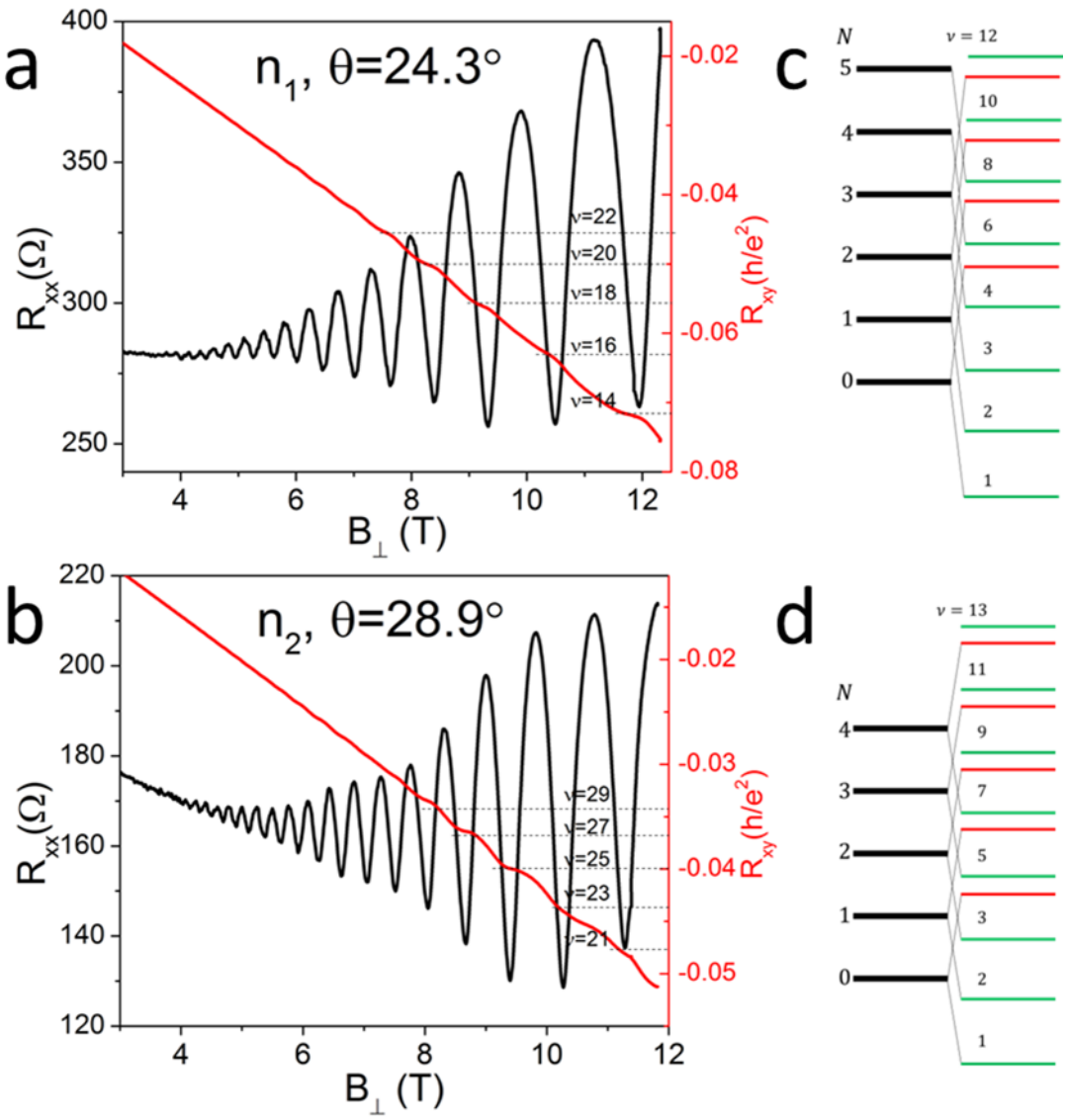

Figure 4: Quantum Hall states at first coincidence angles. (**a,b**) R_{xx} and R_{xy} as a function of B at corresponding first coincidence angles for (**a**) $n_1 = 4.0 \times 10^{12}$ cm^{-2} ($\theta = 24.3°$) and (**b**) $n_2 = 5.7 \times 10^{12}$ cm^{-2} ($\theta = 28.9°$). The QH plateaux in R_{xy} show even and odd sequences in (**a**) and (**b**), respectively. (c,d) Schematic diagrams of LLs at zero tilt angle for (**a**) n_1 and (**b**) n_2. The green and red lines represent spin-down and spin-up states, respectively.